J|A|C|S
ARTICLES
Published on Web 07/18/2006

Lithium Diisopropylamide-Mediated Enolization: Catalysis by Hemilabile Ligands

Antonio Ramirez, Xiufeng Sun, and David B. Collum*

Contribution from the Department of Chemistry and Chemical Biology, Baker Laboratory, Cornell University, Ithaca, New York 14853-1301

Received March 29, 2006; E-mail: dbc6@cornell.edu

Abstract: Structural, kinetic, and computational studies reveal the mechanistic complexities of a lithium diisopropylamide (LDA)-mediated ester enolization. Hemilabile amino ether $MeOCH_2CH_2NMe_2$, binding as an η^1 (ether-bound) ligand in the reactant and as an η^2 (chelating) ligand in the transition structure, accelerates the enolization 10,000-fold compared with *n*-BuOMe. At the onset of the reaction, a dimer-based enolization prevails. As the reaction proceeds, significantly less reactive LDA-enolate mixed dimers appear and divert the reaction through monomer- and mixed dimer-based pathways. The mechanistic and computational investigations lead to a proof-of-principle ligand-catalyzed enolization in which an ancillary ligand allows the catalytic ligand to re-enter the catalytic cycle.

Introduction

Organolithium reagents are prominent in organic chemistry. Given the importance of designer ligands to impart stereo- and regiochemical control,[1] it is curious that ligand-catalyzed reactions are rare.[2] We suspect that many attempts to achieve ligand-based catalysis are thwarted by the occlusion of the catalyst on the lithium salt products and byproducts (eq 1).[3] The problem of occlusion stems, at least in part, from the profound sensitivity of the ligand−lithium interactions to steric effects. If a lithium salt generated during a reaction is less sterically demanding than the starting organolithium reagent, the ligand binds strongly to the product and does not readily re-enter the catalytic cycle.

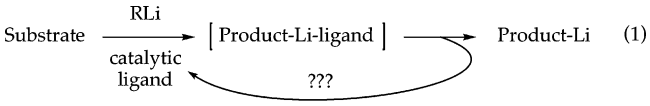

(1)

A few examples of successful ligand-based catalysis shed light on the underlying structural and mechanistic issues that remain largely unresolved. The most prevalent ligand-catalyzed organolithium reactions involve 1,2-additions of alkyllithiums to imines (eq 2).[2a] Mechanistic details are not understood, but the facility of catalysis is easy to rationalize: The inordinately weak coordination of chelating ligands to hindered lithium dialkylamides appears to ensure a facile extrusion of the ligand.[4]

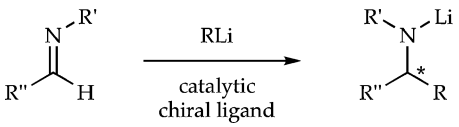

(2)

Tomioka and co-workers have reported ligand-catalyzed 1,4-additions of lithium amides to unsaturated esters (eq 3).[2b] On first inspection, a simple steric model seems inadequate given that lithium enolates appear to be considerably *less* hindered than lithium dialkylamides.[5] However, recent structural studies reveal that β-amino ester enolates can form higher aggregates

(1) Chelating ligands in asymmetric organolithium chemistry: (a) Hodgson, D. M.; Gras, E. *Synthesis* **2002**, 1625. (b) Sibi, M. P.; Manyem, S. *Tetrahedron* **2000**, *56*, 8033. (c) Kobayashi, S.; Ishitani, H. *Chem. Rev.* **1999**, *99*, 1069. (d) Bloch, R. *Chem. Rev.* **1998**, *98*, 1407. (e) Jones C. A. G.; North, M. *Tetrahedron: Asymmetry* **1997**, *8*, 3789. (f) Denmark, S. E.; Nicaise, O. J.-C. *J. Chem. Soc., Chem. Commun.* **1996**, 999. (g) Tomioka, K. *Synthesis* **1990**, 541.

(2) (a) 1,2-Additions to imines: Kizirian, J.-C.; Cabello, N.; Pinchard, L.; Caille, J.-C.; Alexakis, A. *Tetrahedron* **2005**, *61*, 8939; Cointeaux, L.; Alexakis, A. *Tetrahedron: Asymmetry* **2005**, *16*, 925; Hata, S.; Iwasawa, T.; Iguchi, M.; Yamada, K.; Tomioka, K. *Synthesis* **2004**, 1471; Alexakis, A.; Amiot, F. *Tetrahedron: Asymmetry* **2002**, *13*, 2117; Hasegawa, M.; Taniyama, D.; Tomioka, K. *Tetrahedron* **2000**, *56*, 10153; Kambara, T.; Tomioka, K. *Chem. Pharm. Bull.* **1999**, *47*, 720; Inoue, I.; Shindo, M.; Koga, K.; Kanai, M.; Tomioka, K. *Tetrahedron: Asymmetry* **1995**, *6*, 2527; Inoue, I.; Shindo, M.; Koga, K.; Tomioka, K. *Tetrahedron* **1994**, *50*, 4429; Tomioka, K.; Inoue, I.; Shindo, M.; Koga, K. *Tetrahedron Lett.* **1991**, *32*, 3095; For a review, see: Iguchi, M.; Yamada, K.; Tomioka, K. *Topics Organomet. Chem.* **2003**, *5*, 37. (b) Conjugate addition of lithium amides: Doi, H.; Sakai, T.; Iguchi, M.; Yamada, K.; Tomioka, K. *J. Am. Chem. Soc.* **2003**, *125*, 2886. (c) Alkylation of enolates: Imai, M.; Hagihara, A.; Kawasaki, H.; Manabe, K.; Koga, K. *Tetrahedron* **2000**, *56*, 179; Yamashita, Y.; Odashima, K.; Koga, K. *Tetrahedron Lett.* **1999**, *40*, 2803; Imai, M.; Hagihara, A.; Kawasaki, H.; Manabe, K.; Koga, K. *J. Am. Chem. Soc.* **1994**, *116*, 8829; Koga, K. *Pure Appl. Chem.* **1994**, *66*, 1487. (d) Ortholithiations: Slocum, D. W.; Moon, R.; Thompson, J.; Coffey, D. S.; Li, J. D.; Slocum, M. G.; Siegel, A.; Gayton-Garcia, R. *Tetrahedron Lett.* **1994**, *35*, 385. (e) Conjugate addition of lithium thiolates: Nishimura, K.; Tomioka, K. *J. Org. Chem.* **2002,** *67*, 431; Kambara, T.; Tomioka, K. *Chem. Pharm. Bull.* **2000**, *48*, 1577; Tomioka, K.; Okuda, M.; Nishimura, K.; Manabe, S.; Kanai, M.; Nagaoka, Y.; Koga K. *Tetrahedron Lett.* **1998**, *39*, 2141; Nishimura, K.; Ono, M.; Nagaoka, Y.; Tomioka, K. *J. Am. Chem. Soc.* **1997**, *119*, 12974. (f) Carbolithiations: Norsikian, S.; Marek, I.; Normant, J. F. *Tetrahedron Lett.* **1997**, *38*, 7523; Norsikian, S.; Marek, I.; Poisson, J. F.; Normant, J. F. *J. Org. Chem.* **1997**, *62*, 4898; Klein, S.; Marek, I.; Poisson, J. F.; Normant, J. F. *J. Am. Chem. Soc.* **1995**, *117*, 8853; Lautens, M.; Gajda, C.; Chiu, P. *J. Chem. Soc., Chem. Commun.* **1993**, 1193. (g) Wittig rearrangements: Tomooka, K.; Komine, N.; Nakai, T. *Chirality* **2000**, *12*, 505. (h) Nucleophilic aromatic substitutions: Shindo, M.; Koga, K.; Tomioka, K. *J. Am. Chem.* Soc. **1992**, *114*, 8732. (i) Deprotonation of epoxides: Hodgson, D. M.; Lee, G. P.; Marriott, R. E.; Thompson, A. J.; Wisedale, R.; Witherington, J. *J. Chem. Soc., Perkin Trans. 1* **1998**, 2151. (j) Deprotonation of carbamates and phosphine boranes: McGrath, M. J.; O'Brien, P. *J. Am. Chem. Soc.* **2005**, *127*, 16378.

(3) Normant, J. F. *Topics Organomet. Chem.* **2003**, *5*, 287. Wanat, R. A.; Collum, D. B. *J. Am. Chem.* Soc. **1985**, *107*, 2078.

(4) Lucht, B. L.; Bernstein, M. P.; Remenar, J. F.; Collum, D. B. *J. Am. Chem. Soc.* **1996**, *118*, 10707.

10.1021/ja062147h CCC: $33.50

that display little tendency to accept coordinating ligands.[6] Thus, ligand **1** will readily re-enter the catalytic cycle *if* the product of the reaction is prone to form sterically demanding higher aggregates. Unfortunately, product salts are prone to *deaggregate* because they are almost always inductively stabilized relative to the reactants.[7, 8]

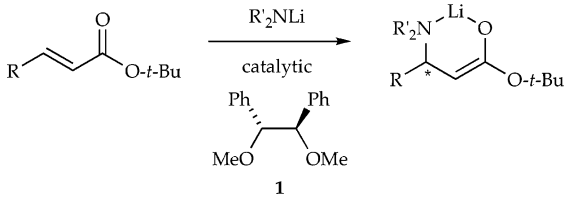

(3)

Koga and co-workers reported asymmetric alkylations of lithium enolates catalyzed by a precious polyamine (eq 4).[2c] Although the coordinating capacity of polyamines and polyethers may be overstated,[4,9] the LiBr formed during the alkylation (and complexed with methyllithium) should have occluded Koga's ligand with a vengeance.[10] We surmise that TMEDA[11] was added to coax the LiBr to release the polyamine ligand.[12] Thus, successful catalysis and high stereocontrol may derive from a transition structure-selective chiral ligand and a LiBr-selective stoichiometric (ancillary) ligand.

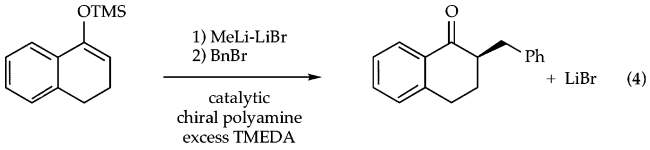

(4)

As a final example, Slocum and co-workers reported that TMEDA can be used catalytically to accelerate *n*-BuLi-mediated ortholithiations (eq 5).[2d] The aggregation state of ortholithiated anisole with added TMEDA is unclear.[13] It seems highly probable, however, that *n*-BuLi−ArLi mixed aggregates are generated during the ortholithiation.[14] Do these mixed aggregates release the ligand efficiently? Do the mixed aggregates effect ortholithiation without dissociation? Mixed aggregation adds another layer of complexity.

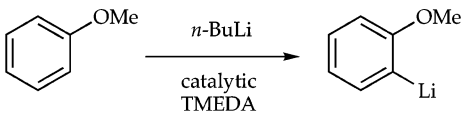

(5)

We describe herein an enolization of ester **2** in which hemilabile[15] amino ether **B** is used catalytically (eq 6). A 10,000-fold acceleration by **B** when compared with isostructural dialkyl ether counterparts underscored potential applications of amino ether-*catalyzed* enolizations.

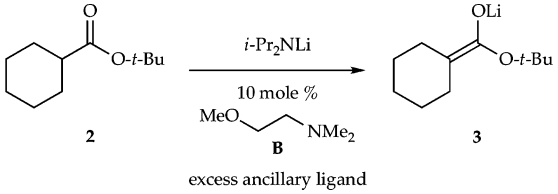

(6)

Our approach to developing a ligand-catalyzed ester enolization from first principles is based on an understanding of the complex reaction coordinates. We began with structural studies of lithium diisopropylamide (LDA) and rate studies showing the mechanism of enolization. As the enolization proceeds, however, the formation of LDA-lithium enolate mixed aggregates is accompanied by changes in mechanism. The ligand-dependent structures and reactivities of these mixed aggregates afford some surprising conclusions about how mixed aggregation influences mechanism. By probing autoinhibition derived from both mixed aggregation and ligand occlusion we have identified a stoichiometric ancillary ligand that facilitates the reentry of amino ether **B** to the catalytic cycle. Computational data juxtaposed with the experimental results fill in experimentally elusive details, and it all coalesces into a self-consistent mechanistic picture.

Results

Lithium Diisopropylamide Solution Structures. Previous investigations have shown that LDA is a disolvated dimer (**4**) in ethereal solvents[16] as well as in a number of amino ethers and diethers.[17c,18] The pronounced preference for the η^1 form with exclusive coordination by a methoxy moiety rather than by a dialkylamino group[17] derives from severe steric congestion within the coordination sphere of the lithium.[8] ^{6}Li and ^{15}N NMR spectra of [^{6}Li,^{15}N]LDA are included in the Supporting Information.

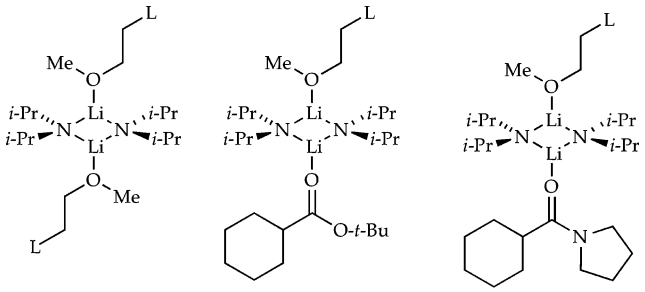

A; L = CH_2CH_3 (*n*-BuOMe)
B; L = NMe_2
C; L = N(*i*-Pr)$_2$

Lithium Diisopropylamide-Substrate Complexation. Detailed rate studies of LDA-mediated enolizations of ester **2** were complicated by exceptionally high rates (vide infra) and partial substrate−LDA complexation. Thus, IR spectra of solutions containing LDA (0.10 M), ester **2** (0.004 M), and ligands **A**−**C** (0.50 M) show absorbances corresponding to free ester (1729

(5) (a) Boche, G.; Langlotz, I.; Marsch, M.; Harms, K. *Chem. Ber.* **1994**, *127*, 2059. (b) Jackman, L. M.; Bortiatynski, J. *Adv. Carbanion Chem.* **1992**, *1*, 45. (c) Williard, P. G. *Comprehensive Organic Synthesis*; Pergamon: New York, 1991; Vol. 1, pp 1−47. (d) Seebach, D. *Angew Chem., Int. Ed. Engl.* **1988**, *27*, 1624. (e) Jastrzebski, J. T. B. H.; van Koten, G.; van de Mieroop, W. F. *Inorg. Chim. Acta* **1988**, *142*, 169.
(6) (a) McNeil, A. J.; Toombes, G. E. S.; Gruner, S. M.; Lobkovsky, E.; Collum, D. B.; Chandramouli, S. V.; Vanasse, B. J.; Ayers, T. A. *J. Am. Chem. Soc.* **2004**, *126*, 16559. (b) McNeil, A. J.; Toombes, G. E. S.; Chandramouli, S. V.; Vanasse, B. J.; Ayers, T. A.; O'Brien, M. K.; Lobkovsky, E.; Gruner, S. M.; Marohn, J. A.; Collum, D. B. *J. Am. Chem. Soc.* **2004**, *126*, 5938.
(7) (a) Reich, H. J.; Goldenberg, W. S.; Sanders, A. W.; Jantzi, K. L.; Tzschucke, C. C. *J. Am. Chem. Soc.* **2003**, *125*, 3509. (b) Reich, H. J.; Goldenberg, W. S.; Gudmundsson, B. Ö.; Sanders, A. W.; Kulicke, K. J.; Simon, K.; Guzei, I. A. *J. Am. Chem. Soc.* **2001**, *123*, 8067.
(8) Lucht, B. L.; Collum, D. B. *Acc. Chem. Res.* **1999**, *32*, 1035.
(9) Remenar, J. F.; Collum, D. B. *J. Am. Chem. Soc.* **1998**, *120*, 4081.
(10) (a) Polt, R.; Seebach, D. *Helv. Chim. Acta* **1987**, *70*, 1930. (b) Wanat, R. A.; Collum, D. B. *J. Am. Chem. Soc.* **1985**, *107*, 2078.
(11) TMEDA = *N*,*N*,*N*′,*N*′-tetramethylethylenediamine.
(12) Collum, D. B. *Acc. Chem. Res.* **1992**, *25*, 448.

Table 1. ^{6}Li and ^{15}N Spectral Data[a,b]

compd	^{6}Li, δ (m, J_{LiN})	^{15}N, δ (m, J_{LiN})
$\mathbf{4}_A$	1.82 (t, 5.0)	73.6 (q, 5.0)
$\mathbf{4}_B$	1.70 (t, 5.1)	69.4 (q, 5.1)[c]
$\mathbf{4}_C$	2.13 (t, 4.8)	73.4 (q, 5.0)
$\mathbf{6}_A$[d]	1.91 (t, 5.0)	73.8 (q, 5.1)
	2.13 (t, 5.2)	
$\mathbf{6}_B$[d]	1.19 (t, 4.8)	69.5 (q, 4.9)[c]
	2.15 (t, 4.8)	
$\mathbf{6}_C$[d]	1.90 (t, 4.9)	73.8 (q, 4.9)
	2.10 (t, 4.8)	
$\mathbf{12}_A$	1.23 (d, 5.1)	73.5 (q, 5.0)
$\mathbf{12}_B$	0.72 (d, 5.1)	73.7 (q, 5.1)
$\mathbf{12}_C$	1.43 (d, 5.1)	
$\mathbf{13}_A$	1.82 (t, 4.7)	71.4 (q, 5.3)
	1.35 (d, 6.2)	
$\mathbf{13}_C$	1.82 (t, 4.9)	72.7 (br m)
	1.22 (d, 6.3)	
$\mathbf{14}_A$	0.50, 0.32, 0.19[e]	
$\mathbf{14}_B$	−0.13[e]	
$\mathbf{14}_C$	−0.10[e]	

[a] All samples were recorded at −90 °C. [b] Spectra were recorded on samples containing 0.13 M total lithium concentration (normality). Coupling constants were measured after resolution enhancement. Multiplicities are denoted as follows: d = doublet, t = triplet, q = quintet, br m = broad multiplet. The chemical shifts are reported relative to 0.3 M ^{6}LiCl/MeOH at −90 °C (0.0 ppm) and neat Me_2NEt (25.7 ppm). All *J* values are reported in Hz. [c] Obscured by another resonance. [d] Recorded at −125 °C. [e] All signals attributed to homonuclear enolate aggregates (**14**) are singlets.

cm^{-1}) *and* LDA-bound ester ($\mathbf{5}_{A-C}$; 1703 cm^{-1}).[19a] The ratios of free and bound ester confirm that the binding constants of ligands **A**−**C** are indistinguishable and that ligands **A**−**C** are η^1 methoxy-bound on dimers **4**−**6**.[17]

We turned to the highly Lewis basic and considerably less-reactive carboxamide **7** as an ester surrogate to control reactant structure (eq 7). IR spectra recorded on solutions containing LDA (0.10 M) and **7** (0.004 M) in the presence of ligands **A**−**C** show absorbances corresponding to LDA-bound carboxamide ($\mathbf{6}_{A-C}$; 1636 cm^{-1})[19a] to the exclusion of free carboxamide (1654 cm^{-1}).[20] NMR spectra recorded on solutions of [^{6}Li,^{15}N]LDA and carboxamide **7** in **A**−**C** reveal, in each case, two ^{6}Li resonances and one ^{15}N resonance emblematic of the dimer-based complexes ($\mathbf{6}_{A-C}$; Table 1).

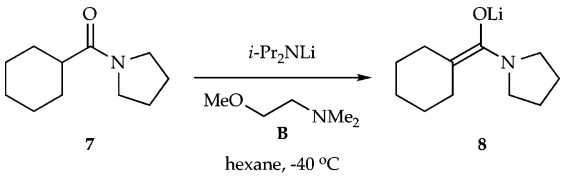

(7)

Kinetics: General. Unsolvated LDA was doubly recrystallized[21] and handled as freshly prepared stock solutions. Pseudo-first-order conditions were established with LDA at normal concentrations (0.05−0.40 M)[22a] by restricting the substrate concentration to 0.004 M. The solvent concentration refers to the concentration of *free* (uncoordinated) donor solvent in hexane cosolvent.[22b] In all cases, loss of starting ester or carboxamide follows a clean first-order decay to five half-lives. The resulting pseudo-first-order rate constants (k_{obsd}) are independent of substrate concentration (0.004−0.04 M). Zeroing the IR baseline and monitoring a second injection of substrate affords no significant change in k_{obsd} (± 10%), showing that autocatalysis, autoinhibition, and other conversion-dependent effects are unimportant under pseudo-first-order conditions. Substantial isotope effects attest to rate-limiting proton transfers. Ligand-dependent relative rate constants are summarized in Table 2. The resulting rate laws and isotope effects are summarized in Table 3.

Table 2. Relative Rate Constants for the LDA-Mediated Enolization of Ester **2** ($k_{rel}1$, eq 6) and Carboxamide **7** ($k_{rel}2$, eq 7) in the Presence of Hemilabile Ligands

ligand[a]	$k_{rel}1$[b]	$k_{rel}2$[c]
A; *n*-BuOMe	1	1
B; $MeOCH_2CH_2NMe_2$	10,000	30
C; $MeOCH_2CH_2N(i\text{-}Pr)_2$	10	3

[a] [Ligand] = 0.5 M. [b] Measured at −78 °C. [c] Measured at −30 °C.

Table 3. Summary of Rate Studies for the LDA-Mediated Enolization of Carboxamide **7** (eq 7)

entry	temp (°C)	ligand	LDA[a] order	ligand order	k_H/k_D
1	0	A	0	0	6.2 ± 0.7
2	−40	B	0	0	7.5 ± 0.5
3	−30	C	0	0	6.3 ± 0.3

[a] [Ligand] = 0.5 M.

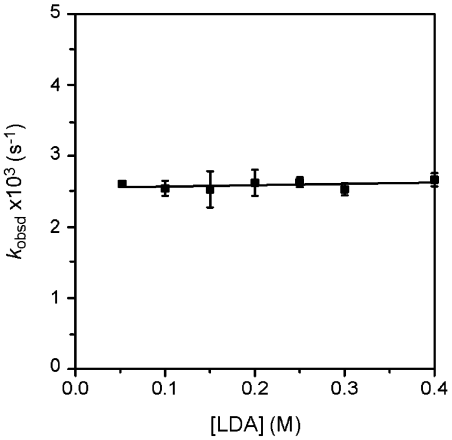

Figure 1. Plot of k_{obsd} vs [LDA] in *n*-BuOMe (0.5 M) and hexane cosolvent for the enolization of **7** (0.004 M) at 0 °C. The curve depicts an unweighted least-squares fit to $k_{obsd} = k$ [LDA] + k' ($k = (2 \pm 2) \times 10^{-4}$, $k' = (2.5 \pm 0.1) \times 10^{-3}$).

Lithium Diisopropylamide-Dimer-Derived Enolization. We routinely use *n*-BuOMe as a benchmark for comparison with hemilabile amino ethers and diethers.[17] Monitoring LDA-mediated enolizations of carboxamide **7** in *n*-BuOMe at 0 °C using in situ IR spectroscopy reveals that LDA-carboxamide complex $\mathbf{6}_A$ undergoes a first-order decay that is independent of the concentrations of both excess LDA and *n*-BuOMe (Figures 1 and 2). The idealized rate law (eq 8) and substantial isotope effects are consistent with a dimer-based pathway depicted generically in eq 9. An analogous mechanism was observed for LDA/*t*-BuOMe-mediated ester enolizations.[19a] Open dimer-based transition structure **9A** is supported by

(13) (a) Boman, A.; Johnels, D. *Magn. Reson. Chem.* **2000**, *38*, 853. (b) Reich, H. J.; Sikorski, W. H.; Gudmundsson, B. O.; Dykstra, R. R. *J. Am. Chem. Soc.* **1998**, *120*, 4035. (c) Harder, S.; Boersma, J.; Brandsma, L.; Van Mier, G, P. M.; Kanters, J. A. *J. Organomet. Chem.* **1989**, *364*, 1.
(14) Gossage, R. A.; Jastrzebski, J. T. B. H.; van Koten, G. *Angew. Chem., Int. Ed.* **2005**, *44*, 1448.
(15) For reviews of hemilabile ligands, see: (a) Braunstein, P.; Naud, F. *Angew. Chem., Int. Ed.* **2001**, *40*, 680. (b) Slone, C. S.; Weinberger, D. A.; Mirkin, C. A. *Progr. Inorg. Chem.* **1999**, *48*, 233. (c) Lindner, E.; Pautz, S.; Haustein, M. *Coord. Chem. Rev.* **1996**, *155*, 145. (d) Bader, A.; Lindner, E. *Coord. Chem. Rev.* **1991**, *108*, 27.
(16) Collum, D. B. *Acc. Chem. Res.* **1993**, *26*, 227.
(17) (a) Remenar, J. F.; Collum, D. B. *J. Am. Chem. Soc.* **1997**, *119*, 5573. (b) Ramirez, A.; Collum, D. B. *J. Am. Chem. Soc.* **1999**, *121*, 11114. (c) Ramirez, A.; Lobkovsky, E.; Collum, D. B. *J. Am. Chem. Soc.* **2003**, *125*, 15376.

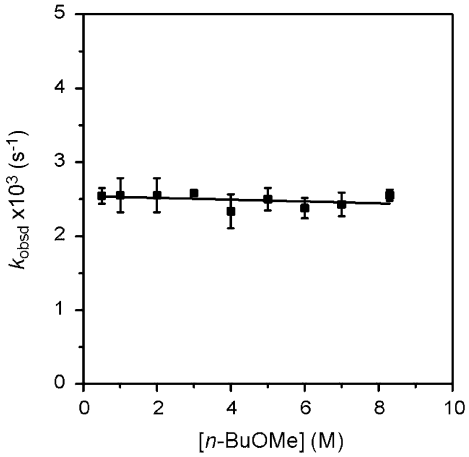

Figure 2. Plot of k_{obsd} vs [*n*-BuOMe] in hexane cosolvent for the enolization of **7** (0.004 M) by LDA (0.10 M) at 0 °C. The curve depicts an unweighted least-squares fit to $k_{obsd} = k$ [*n*-BuOMe] + k' ($k = (-1 \pm 1) \times 10^{-5}$, $k' = (2.5 \pm 0.1) \times 10^{-3}$).

spectroscopically[23] and crystallographically characterized[24] lithium amide open dimers as well as computational data.[25]

$$-\mathrm{d}[\mathbf{6}]/\mathrm{d}t = k'[\mathbf{6}] \quad (8)$$

$$(i\text{-Pr}_2\text{NLi})_2(\text{ligand})(\mathbf{7}) \rightarrow \text{enolate} \quad (9)$$
$$(\text{e.g., } \mathbf{6})$$

The enolization of **7** using LDA/**B** mixtures is 30 times faster than that using LDA/*n*-BuOMe mixtures. Because *n*-BuOMe and **B** bind equivalently in the dimeric LDA,[17a] the higher rate for LDA/**B** compared with that for LDA/*n*-BuOMe shows that ligand **B** is chelating in the transition structure. The loss of complex $\mathbf{6}_B$ in $MeOCH_2CH_2NMe_2$/hexane mixtures at −40 °C affords a zeroth-order dependence on both LDA and amino ether **B**, consistent with the idealized rate law in eq 8, the mechanism described by eq 9, and open-dimer-based transition structure $\mathbf{10}_B$.

As part of efforts to achieve and understand a ligand-*catalyzed* enolization (vide infra) we examined ligands that might displace ligand **B** from the homo- or heteroaggregated products without accelerating the reaction. We surveyed weakly chelating diethers and amino ethers that previously showed little capacity to accelerate LDA-mediated reactions[17a,c] and ultimately focused on amino ether **C**.[26] Ligand **C** only marginally accelerates the enolization of **7** (Table 2) when compared with *n*-BuOMe. The rate constants measured at −30 °C are independent of LDA and ligand concentrations (Table 3) and are consistent with the idealized rate law in eq 8 and the general mechanism described by eq 9. The importance of ligand **C** for occluding the enolate products without accelerating the enolization is detailed below.

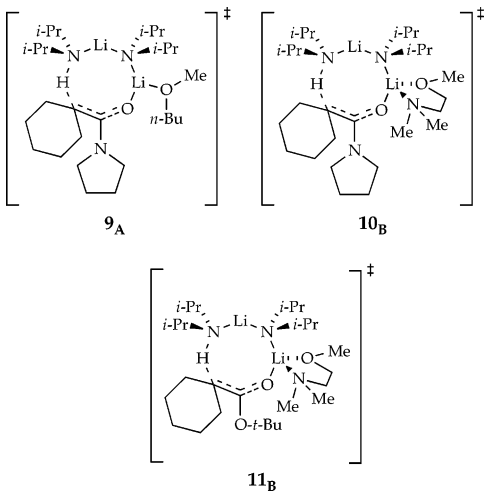

Recall that LDA/**B**-mediated enolizations of ester **2** are difficult to study because of both excessively high rates even at −78 °C and partial complexation to LDA at higher ligand concentrations. One might question, however, whether carboxamide **7** is a valid surrogate of ester **2** owing to its measurably different rate behavior. We obtained support for the analogy from rate studies of enolization of ester **2** at low (<0.5 M)[22] concentrations of amino ether **C** wherein $\mathbf{6}_C$ is formed nearly quantitatively. Under these conditions, the enolization rates are independent of the concentrations of either ligand **C** or LDA, consistent with a dimer-based mechanism.[19a,27] All subsequent studies described below used ester **2**.

Mixed Aggregation and Autoinhibition. To understand ligand-catalyzed enolizations, it is necessary to understand the mixed aggregation and autoinhibition that arise during the course of an enolization using equimolar concentrations of substrate and LDA.[19b]

Autoinhibition can derive from a number of sources including (1) the formation of relatively unreactive mixed aggregates (heteroaggregates), and (2) strong binding of either the substrate (ester **2**) or the catalyst (ligand **B**) to homo- or heteroaggregated enolate. This section focuses on the potentially baffling ligand-dependent mixed aggregate equilibria described by eqs 11−16, which underlie ligand-derived catalysis. It is instructive at the outset to note that (1) the mixed aggregate equilibria shift to maximize the number of chelated lithiums, (2) the existence of chelation is dictated by congestion within the aggregates, and (3) the enolate subunit is less sterically demanding than the *i*-Pr_2NLi moiety, resulting in steric demands that follow the order:

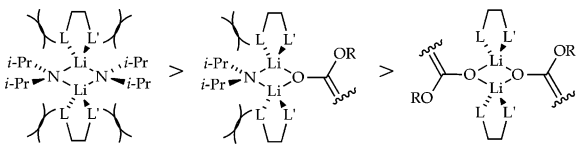
(10)

Enolization of ester **2** by 1.0 equiv of LDA at −25 °C in 1.0 M *n*-BuOMe/hexane stalls at approximately 50% conversion. The incomplete reaction is certainly *not* owing to occlusion of the *n*-BuOMe because the *n*-BuOMe is present in considerable excess. Similarly, tenacious coordination of the starting ester

(18) Remenar, J. F.; Lucht, B. L.; Collum, D. B. *J. Am. Chem. Soc.* **1997**, *119*, 5567.
(19) (a) Sun, X.; Collum, D. B. *J. Am. Chem. Soc.* **2000**, *122*, 2452. (b) Sun, X.; Collum, D. B. *J. Am. Chem. Soc.* **2000**, *122*, 2459. (c) Sun, X.; Kenkre, S. L.; Remenar, J. F.; Gilchrist, J. H.; Collum, D. B. *J. Am. Chem. Soc.* **1997**, *119*, 4765.
(20) The structure of LDA-bound carboxamide **6** has been confirmed by ^{6}Li and ^{15}N NMR spectroscopy, see ref 19a. See also Supporting Information.
(21) Bernstein, M. P.; Romesberg, F. E.; Fuller, D. J.; Harrison, A. T.; Williard, P. G.; Liu, Q. Y.; Collum, D. B. *J. Am. Chem. Soc.* **1992**, *114*, 5100.
(22) (a) "[LDA]" and "[enolate]" refers to the concentration of the monomer subunit (normality). (b) This ligand concentration refers to *free* donor solvent in hexane cosolvent.
(23) (a) Remenar, J. F.; Lucht, B. L.; Kruglyak, D.; Romesberg, F. E.; Gilchirst, J. H.; Collum, D. B. *J.* Org. *Chem.* **1997**, *62*, 5748. (b) Romesberg, F. E.; Collum, D. B. *J. Am. Chem. Soc.* **1992**, *114*, 2112. (c) Romesberg, F. E.; Gilchrist, J. H.; Harrison, A. T.; Fuller, D. J.; Collum, D. B. *J. Am. Chem. Soc.* **1991**, *113*, 5751.
(24) Williard, P. G.; Liu, Q.-Y. *J. Am. Chem. Soc.* **1993**, *115*, 3380.

to the products of the reaction can be excluded because IR spectroscopy shows that the ester is largely (>95%) uncomplexed. The elimination of these possibilities leaves mixed aggregation as the culprit.

Indeed, ^{6}Li and ^{15}N NMR spectroscopic analyses on reactions using 1.0 equiv of [^{6}Li,^{15}N]LDA show that reactions at <50% conversion contain mixed dimer $\mathbf{12}_A$ and mixed trimer $\mathbf{13}_A$ to the exclusion of the homoaggregated enolate (eq 11; Table 1).

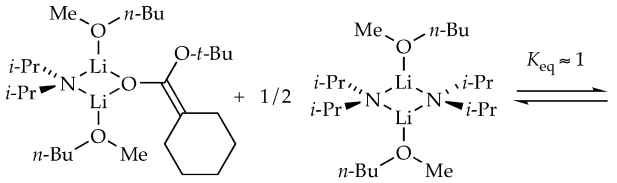

$\mathbf{12}_A$ $\mathbf{4}_A$

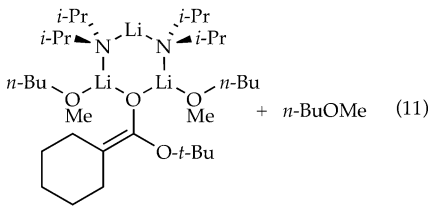

(11)

$\mathbf{13}_A$

The implicit partial solvation of $\mathbf{13}_A$ (<1.0 solvent per Li) is supported by computational studies and is consistent with extensive evidence of partial solvation of cyclic trimers.[28] Importantly, the dimer/trimer mixture is emblematic of mixed aggregates solvated by nonchelating ligands.

As the reaction reaches 50% conversion, mixed dimer $\mathbf{12}_A$ becomes the only enolate-containing form. The strong preference for mixed dimerization described by eq 12 was previously noted for enolizations by LDA/*t*-BuOMe.[19]

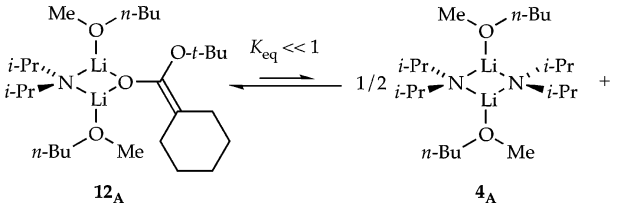

$\mathbf{12}_A$ $\mathbf{4}_A$

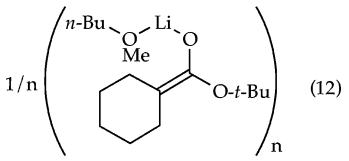

(12)

$\mathbf{14}_A$

Enolization of ester **2** by 1.0 equiv of LDA at −78 °C in a mixture of **B** (11.0 equiv) and hexane proceeds to 50% conversion almost instantaneously and then stalls abruptly. The enolization proceeds to full conversion by adding a second equivalent of LDA. NMR spectroscopic evidence that dimer $\mathbf{12}_B$ contains ligand **B** in a chelated form stems from several structural effects observed using LDA/**B** that are *not* observed using LDA/*n*-BuOMe: (1) There is no observable mixed trimer ($\mathbf{13}_B$) even with excess LDA, attesting to disproportionate stabilization of the dimer (eq 13); (2) the unreacted ester is >95% uncoordinated at 50% conversion even at low ligand concentrations, attesting to an inordinately strong binding of **B** to $\mathbf{12}_B$; and (3) the ^{13}C NMR spectra of mixed dimer $\mathbf{12}_B$ or homoaggregated dimer $\mathbf{14}_B$ with excess **B** at −125 °C reveal free and bound ligand resonances, a phenomenon that is highly characteristic of bifunctional ligands and rarely observed with simple ethereal ligands.[4,29] The trans dispositions of the two Me_2N moieties in dimers $\mathbf{12}_B$ and $\mathbf{14}_B$ (as drawn) minimize steric interactions and receive support from density functional theory (DFT) calculations (vide infra).

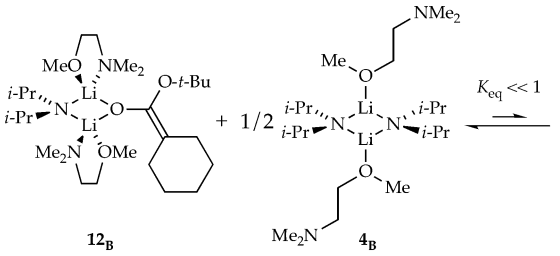

$\mathbf{12}_B$ $\mathbf{4}_B$

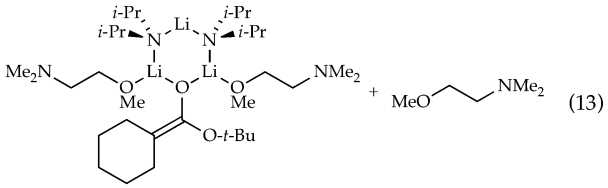

(13)

$\mathbf{13}_B$
(not observed)

As noted above, enolizations of ester **2** under pseudo-first-order conditions by LDA/**C** are, in some respects, indistinguishable from those by LDA/*n*-BuOMe mixtures: The stabilization of the transition structures by chelation is limited. Moreover, enolizations using 1.0 equiv of LDA at <50% conversion afford mixtures of heteroaggregated dimers $\mathbf{12}_C$ and trimer $\mathbf{13}_C$ (eq 15). These enolizations also contain unreacted ester **2** in both free and bound forms. There are, however, two behaviors that distinguish hindered bifunctional ligand **C** from either *n*-BuOMe or amino ether **B**: (1) Enolizations taken to 50% conversion contain considerable concentrations of homoaggregated LDA dimer $\mathbf{4}_C$ and homoaggregated lithium enolate $\mathbf{14}_C$ (eq 16), suggesting inordinate stabilization of the enolate dimer by chelation, and (2) autoinhibition is considerably *less* pronounced for LDA/**C**-mediated enolizations taken beyond 50% conversion, consistent with the marginal occlusion of the homoaggregated LDA dimer through mixed aggregation. Both observations are consistent with chelation of *only* uncongested homoaggregated enolate dimer $\mathbf{14}_C$, leaving homoaggregated LDA dimer $\mathbf{4}_C$ available for enolization.

(25) (a) Romesberg, F. E.; Collum, D. B. *J. Am. Chem. Soc*. **1995**, *117*, 2166. (b) Romesberg, F. E.; Collum, D. B. *J. Am. Chem. Soc*. **1994**, *116*, 9187. (c) Romesberg, F. E.; Bernstein, M. P.; Gilchrist, J. H.; Harrison, A. T.; Fuller, D. J.; Collum, D. B. *J. Am. Chem. Soc.* **1993**, *115*, 3475. (d) Romesberg, F. E.; Collum, D. B. *J. Am. Chem. Soc.* **1992**, *114*, 2112. (e) Henderson, K. W.; Dorigo, A. E.; Liu, Q.-Y.; Williard, P. G. *J. Am. Chem. Soc.* **1997**, *119*, 11855.

(26) The results using $MeOCH_2CH_2O$-*t*-Bu instead of **C** to promote catalysis by ligand **B** were qualitatively similar. Although the basal reactivity in $MeOCH_2CH_2O$-*t*-Bu is lower, the rate of **B**-catalyzed enolization in its presence is lower as well. This is consistent with $MeOCH_2CH_2O$-*t*-Bu being inferior to **C** as a chelating ligand for both the rate-limiting transition structure as well as the resulting mixed aggregate.

(27) Invariant rates (±10%) observed using 0.9−1.5 equiv of amino ether **C** per lithium revealed no evidence of an inverse-dependence on solvent, consistent with an LDA-ester complex.

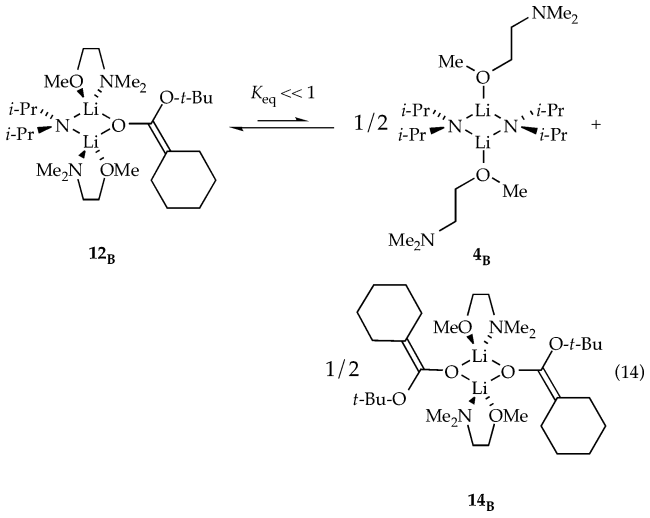

$\mathbf{12_B}$ $\mathbf{4_B}$ $\mathbf{14_B}$

It is prudent to summarize points that are central to the subsequent discussion of catalysis by amino ether **B** as follows: (1) Enolizations of ester **2** by 1.0 equiv of LDA stall at 50% conversion owing to the intervention of mixed aggregates; (2) bifunctional ligand **B** forms stable chelates of mixed dimer $\mathbf{12_B}$ with consequent stabilization of $\mathbf{12_B}$ relative to the mixed trimer (eq 13) as well as the homoaggregates (eq 14); (3) hindered bifunctional ligand **C** shows no capacity to chelate either LDA homodimer $\mathbf{4_C}$ (eq 15)

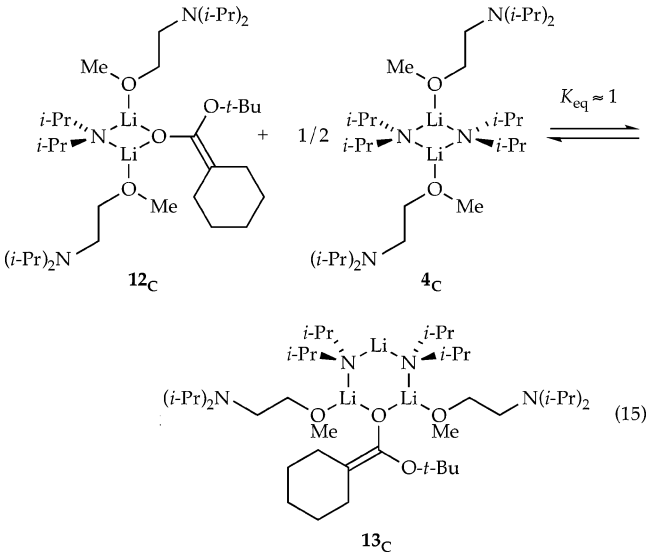

$\mathbf{12_C}$ $\mathbf{4_C}$ $\mathbf{13_C}$

or mixed dimer $\mathbf{12_C}$ (eq 16), but ligand **C** appears to chelate the homoaggregated enolate dimer with consequent displacement of the heteroaggregate-homoaggregate equilibrium in eq 16 toward the homoaggregates.

Mixed Dimer-Derived Enolizations. The previous rate studies precluded conversion-dependent effects of mixed aggregates formed during the reaction by using an excess of LDA (0.05−0.40 M)[22] (compared with the ester concentration [≤0.004 M]). However, standard conditions used in preparative-scale enolizations use nearly equimolar concentrations of LDA and substrate. The next step toward establishing catalysis by hemilabile amino ether **B** required an understanding of the mechanism(s) of enolization when mixed dimer $\mathbf{12_B}$ is the dominant form (eq 17).

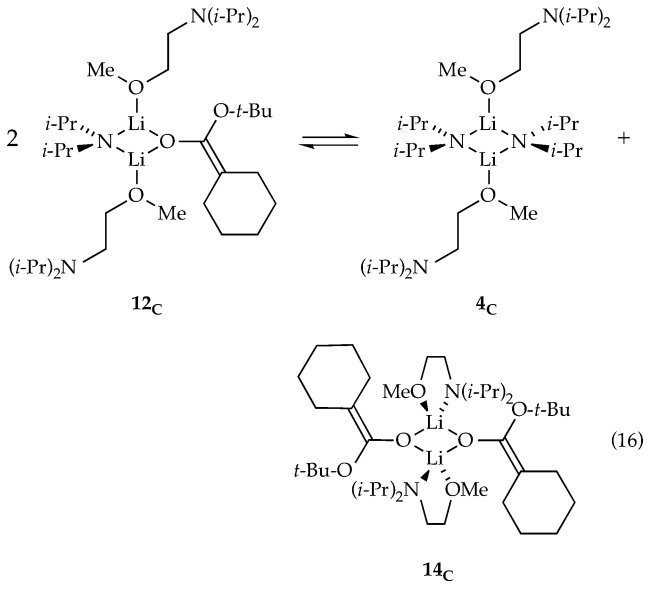

$\mathbf{12_C}$ $\mathbf{4_C}$ $\mathbf{14_C}$

Stock solutions of mixed dimer $\mathbf{12_B}$ were prepared from recrystallized LDA and recrystallized enolate **3**. Pseudo-first-order conditions were achieved by setting the initial concentration of ester at 0.002 M. Enolate **3** was maintained in 0.005 M excess to the concentration of mixed dimer $\mathbf{12_B}$ to ensure the absence of appreciable concentrations of free LDA. The enolizations were monitored using in situ IR spectroscopy by following the loss of free ester (1729 cm^{-1}) at −60 °C. A large isotope effect ($k_H/k_D = 17 \pm 2$)[30] is consistent with a rate-limiting proton transfer. Although the enolization of ester **2** by mixed dimer $\mathbf{12_B}$ is slow compared to that by $\mathbf{5_B}$, enolizations by mixed dimer $\mathbf{12_B}$ are approximately 50-fold faster than those using *n*-BuOMe-solvated mixed dimer $\mathbf{12_A}$.

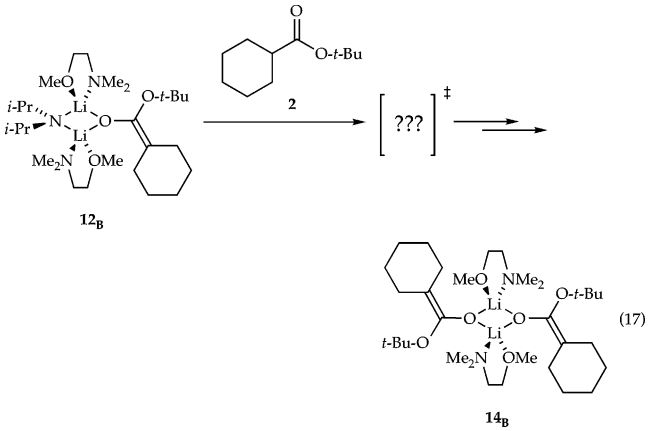

$\mathbf{12_B}$ $\mathbf{14_B}$

The enolization displays an inverse-fractional-order dependence on enolate $\mathbf{14_B}$ that asymptotically approaches a nonzero limiting rate at high enolate concentration[22] (Figure 3) implicating a nondissociative mixed dimer-based pathway at all enolate concentrations and a dissociative LDA-monomer-based pathway at low enolate concentration. We also observe a first-order dependence on mixed dimer $\mathbf{12_B}$ (Figure 4) at high (constant) enolate concentration and a zeroth-order dependence on the

(28) (a) Rutherford, J. L.; Collum, D. B. *J. Am. Chem. Soc.* **2001**, *123*, 199. (b) Rutherford, J. L.; Collum, D. B. *J. Am. Chem. Soc.* **1999**, *121*, 10198.
(29) Hoffmann, D.; Collum, D. B. *J. Am. Chem. Soc.* **1998**, *120*, 5810.

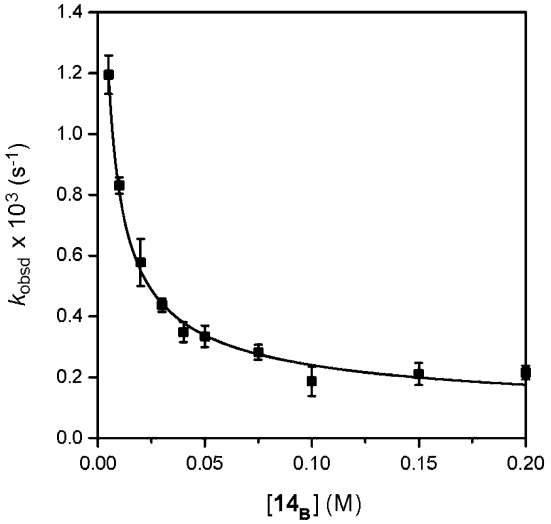

Figure 3. Plot of k_{obsd} vs $[\mathbf{14}_B]^{22}$ in $MeOCH_2CH_2NMe_2$ (0.5 M) and hexane cosolvent for the enolization of ester **2** (0.002 M) by mixed dimer $\mathbf{12}_B$ (0.05 M) at −60 °C. The curve depicts the result of an unweighted least-squares fit to $k_{obsd} = k\,[\mathbf{14}_B]^n + k'$ ($k = (5 \pm 2) \times 10^{-5}$, n = −0.61 ± 0.07, $k' = (5 \pm 5) \times 10^{-5}$).

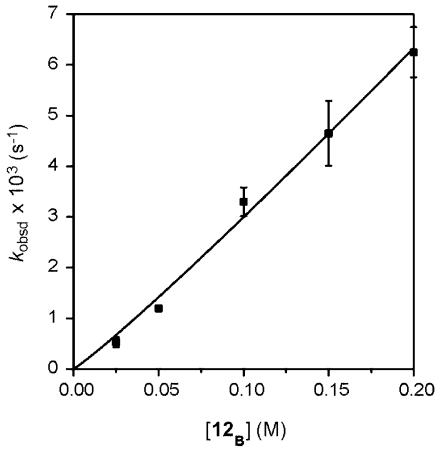

Figure 4. Plot of k_{obsd} vs $[\mathbf{12}_B]$ in $MeOCH_2CH_2NMe_2$ (0.5 M) and hexane cosolvent for the enolization of ester **2** (0.002 M) at −60 °C. The curve depicts the result of an unweighted least-squares fit to $k_{obsd} = k\,[\mathbf{12}_B]^n$ ($k = (3.6 \pm 0.5) \times 10^{-2}$, $n = 1.1 \pm 0.1$.

concentration of ligand **B** under all conditions (Figure 5). Taken together, the reaction orders reveal the monomer-based pathway as described by eqs 18−20 and a mixed dimer-based pathway described by eqs 21 and 22. Guided by computational studies (vide infra), we determined that the data are consistent with monomer-based transition structure $\mathbf{15}_B$ and mixed dimer-based transition structure $\mathbf{16}_B$.

$$-d[\mathbf{2}]/dt = k'\,[\mathbf{B}]^0[\mathbf{12}_B][\text{ester}]\{[\text{enolate}]^{-1/2} + [\text{enolate}]^0\} \quad (18)$$

Monomer-Based Enolization:

$$(i\text{-}Pr_2NLi)(\text{enolate})(\mathbf{B})_2 + \mathbf{2} \rightleftharpoons (i\text{-}Pr_2NLi)(\mathbf{B})(\mathbf{2}) + 1/2\ (\text{enolate})_2(\mathbf{B})_2 \quad (19)$$

(e.g., $\mathbf{12}_B$) (e.g., $\mathbf{14}_B$)

$$(i\text{-}Pr_2NLi)(\mathbf{B})(\mathbf{2}) \rightarrow \text{enolate} \quad (20)$$

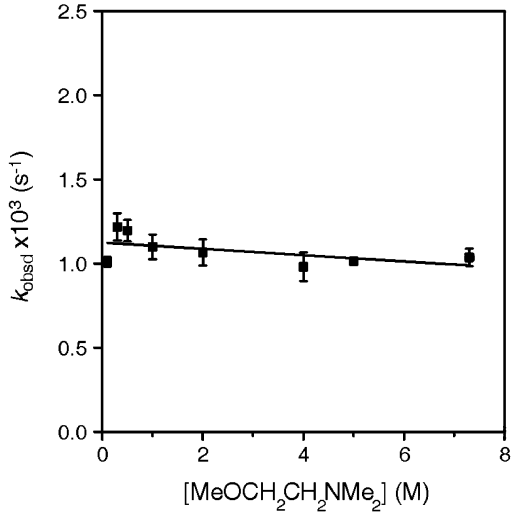

Figure 5. Plot of k_{obsd} vs $[MeOCH_2CH_2NMe_2]$ in hexane cosolvent for the enolization of ester **2** (0.002 M) by mixed dimer $\mathbf{12}_B$ (0.05 M) at −60 °C in the presence of excess enolate $\mathbf{14}_B$ (0.005 M). The curve depicts an unweighted least- squares fit to $k_{obsd} = k\,[MeOCH_2CH_2NMe_2] + k'$ ($k = (-1 \pm 1) \times 10^{-5}$, $k' = (1.1 \pm 0.1) \times 10^{-3}$).

Mixed Dimer-Based Enolization:

$$(i\text{-}Pr_2NLi)(\text{enolate})(\mathbf{B})_2 + \mathbf{2} \rightleftharpoons (i\text{-}Pr_2NLi)(\text{enolate})(\mathbf{B})_2(\mathbf{2}) \quad (21)$$

(e.g., $\mathbf{12}_B$)

$$(i\text{-}Pr_2NLi)(\text{enolate})(\mathbf{B})_2(\mathbf{2}) \rightarrow \text{enolate} \quad (22)$$

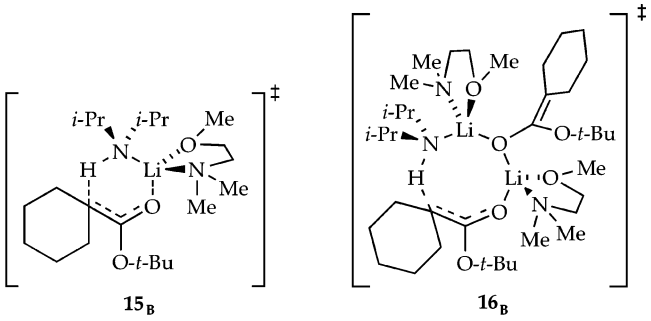

$\mathbf{15_B}$ $\mathbf{16_B}$

Ligand-Catalyzed Enolization. We are now poised to describe a ligand-*catalyzed* enolization through a series of observations. Adding ester **2** (0.05 M) to a solution of LDA (0.10 M, 2.0 equiv) in hexane containing excess *n*-BuOMe (1.0 M) at −78 °C affords no measurable enolization. Subsequent addition of ligand **B** (0.01 M, 0.2 equiv relative to **2**) causes a rapid enolization that stalls at 10% conversion (Figure 6, curve A). The 10% conversion with 20 mol % added **B** is fully consistent with the occlusion of 2 equiv of **B** for each equivalent of enolate generated owing to the formation of doubly chelated mixed aggregate $\mathbf{12}_B$.

We sought a cosolvent with a disproportionately greater affinity for the products than for the transition structure so as to displace ligand **B** from the product for the reentry into the catalytic cycle without the cosolvent eliciting enolization independently. Surveying a number of sterically congested amino ethers and diethers revealed that amino ether **C** satisfied both requirements. Adding ester **2** (0.05 M) to LDA (0.10 M, 2.0 equiv) in hexane

(30) k_H/k_D was determined using **2** and **2**-d_1 (0.002 M), $\mathbf{12}_B$ (0.050 M), and ligand **B** (0.50 M) in hexane cosolvent at −60 °C.

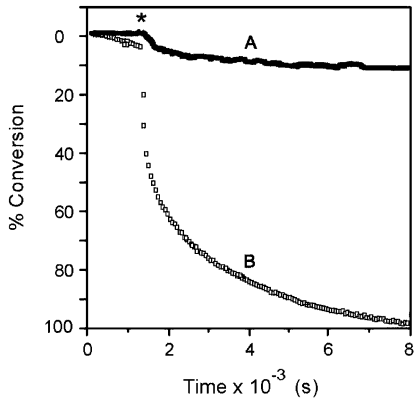

Figure 6. Plot of the percent conversion for the enolization of ester **2** (0.05 M) by LDA (0.1 M) at −78 °C in hexane containing: (A, ■) *n*-BuOMe (1.0 M); (B, □) $MeOCH_2CH_2N(i\text{-}Pr)_2$ (1.0 M). The asterisk indicates the addition of 0.2 equiv of ligand **B** relative to ester **2**.

Chart 1

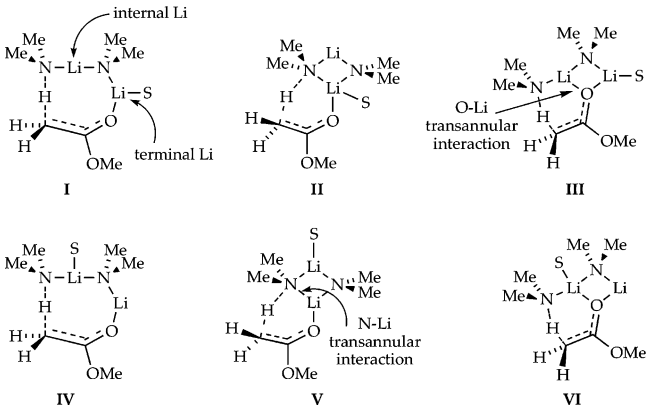

containing excess amino ether **C** (1.0 M) at −78 °C results in a low basal reactivity. Subsequent addition of ligand **B** (0.01 M, 0.2 equiv relative to **2**) causes a 40-fold rate acceleration that persists to >95% conversion (Figure 6, curve B). The concentration of ligand can be reduced to 10 mol % relative to ester, and the reaction still attains **B**-catalyzed enolization to full conversion albeit at a marginally reduced rate.[26]

Computational Studies on Dimer-Based Enolizations. Ester enolizations mediated by LDA dimers were investigated using the density functional theory (B3LYP method and the 6-31G-(d) basis set) available in Gaussian 03.[31] Me_2NLi and $MeCO_2$-Me were used as models for LDA and ester **2**, respectively. *n*-BuOMe and η^1-bound ligand **B** are modeled by Me_2O to simplify conformational effects.[17c] Legitimate saddle points were shown by the existence of a single imaginary frequency. Intrinsic reaction coordinate (IRC) analyses verified that transition structures corresponded to enolizations.

We examined dimer-based transition structures **I**−**VI** (Chart 1), in which the solvent and substrate are placed on the lithium bearing only one coordinated amide fragment (the so-called terminal lithium) or on the lithium flanked by two amide

Chart 2

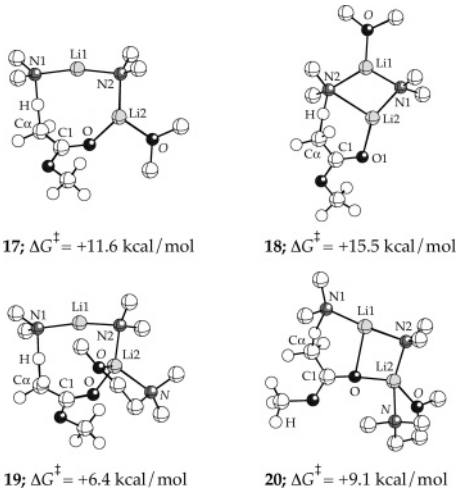

Chart 3. Calculated Reaction Coordinate for the Enolization of $MeCO_2Me$ by $(Me_2NLi)_2/Me_2O$.

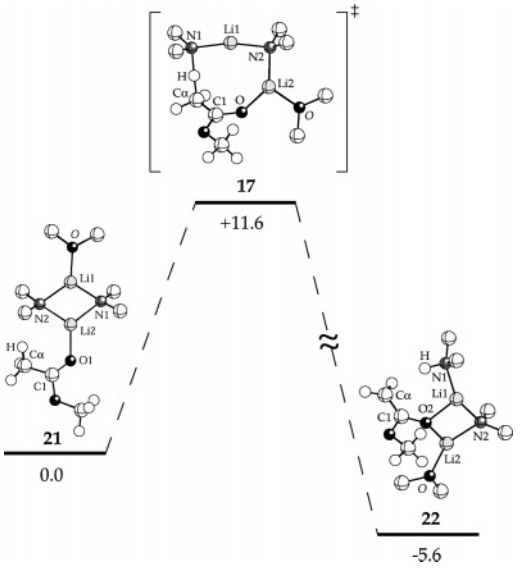

fragments (the internal lithium). The structural types also differ owing to the presence or absence of transannular interactions.[32] Selected bond lengths and angles for transition structures **17**−**20** (Chart 2) are listed in the Supporting Information. The reaction coordinates with relative energies (kcal/mol) are summarized in Charts 3 and 4. Considerable additional data are archived in the Supporting Information.

$(Me_2NLi)_2/Me_2O/MeCO_2Me$. Focusing on geometries **I**−**VI** for ester enolization, we located only transition structures **17** and **18** (Chart 2). The reaction coordinate is summarized in Chart 3. The most stable transition structure **17** corresponds to a type **I** open dimer with coordination of both the substrate and the solvent at the terminal lithium. An IRC calculation shows that

(31) Frisch, M. J. et al. *Gaussian 03*, revision B.04; Gaussian, Inc.: Wallingford, CT, 2004.

(32) (a) Haeffner, F.; Sun, C.; Williard, P. G. *J. Am. Chem. Soc.* **2000**, *122*, 12542. (b) Koch, R.; Wiedel, B.; Anders, E. *J. Org. Chem.* **1996**, *61*, 2523. (c) Henderson, K. W.; Dorigo, A. E.; Liu, Q.-Y.; Williard, P. G.; Schleyer, P. v. R.; Bernstein, P. R. *J. Am. Chem. Soc.* **1996**, *118*, 1339. (d) Nakamura, M.; Nakamura, E. *J. Chem. Soc., Faraday Trans.* **1994**, 1789. (e) Nakamura, M.; Nakamura, E. *J. Am. Chem. Soc.* **1993**, *115*, 11016. (f) Schleyer, P. v. R.; Kaufmann, E. *J. Am. Chem. Soc.* **1985**, *107*, 5560.

(33) (a) Armstrong, D. R.; Carstairs, A.; Henderson, K. W. *Organometallics* **1999**, *18*, 3589. (b) Wanat, R. A.; Collum, D. B.; Van Duyne, G.; Clardy, J.; DePue, R. T. *J. Am. Chem. Soc.* **1986**, *108*, 3415.

(34) (a) Kim, Y.-J.; Streitwieser, A. *Org. Lett.* **2002**, *4*, 573. (b) Flinois, K.; Yuan, Y.; Bastide, C.; Harrison-Marchand, A.; Maddaluno, J. *Tetrahedron* **2002**, *58*, 4707. (c) Matsuo, J.; Odashima, K.; Kobayashi, S. *Org. Lett.* **1999**, *1*, 345. (d) Goto, M.; Akimoto, K.; Aoki, K.; Shindo, M.; Koga, K. *Tetrahedron Lett.* **1999**, *40*, 8129. (e) Uragami, M.; Tomioka, K.; Koga, K. *Tetrahedron: Asymmetry* **1995**, *6*, 701. (f) Hall, P. L.; Gilchrist, J. H.; Harrison, A. T.; Fuller, D. J.; Collum, D. B. *J. Am. Chem.* Soc. **1991**, *113*, 9575.

Chart 4. Calculated Reaction Coordinate for the Enolization of $MeCO_2Me$ by $(Me_2NLi)_2/MeOCH_2CH_2NMe_2$.

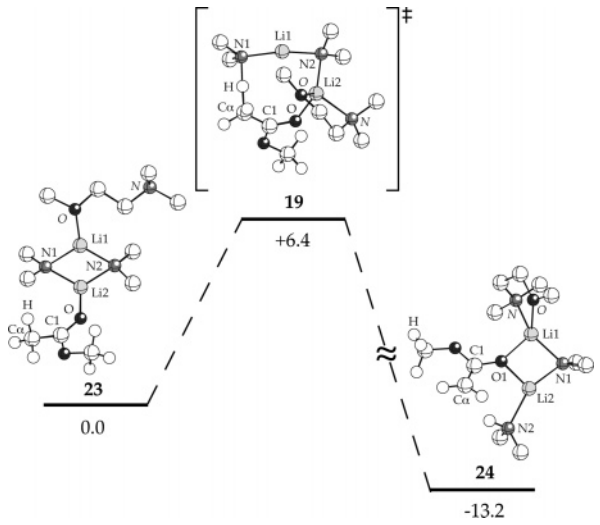

17 proceeds to Me_2NH-solvated[33] mixed dimer **22**.[34,35] The less stable transition structure, **18**, has a transannular N−Li interaction and a solvated internal lithium, suggesting a hybrid of limiting geometries **IV** and **V** (Chart 1). Transition structure **18** also shows a close H−Li contact reminiscent of previously studied agostic interactions.[36] The higher stability of **17** compared to **18** is in agreement with previous semiempirical computations of open dimers and open dimer-based transition structures.[25a,b] The amide fragment in **17** displays N−Li−N and Li−N−Li angles and interatomic bond distances that are nearly equal to those found by Williard and Liu in the crystal structure of an LiTMP open dimer.[24]

$(Me_2NLi)_2/MeOCH_2CH_2NMe_2/MeCO_2Me$. The reaction coordinate for enolizations using ligand **B** is summarized in Chart 4. Open dimer-like type **I** transition structure **19** is more stable than type **II** transition structure **20**. An IRC calculation showed that mixed dimer **24** is the first stable intermediate following open dimer-based transition structure **19**. The approximately 5 kcal/mol lower $\Delta G^{\ddagger}$ using ligand **B** compared with Me_2O concurs with experiments showing 10,000-fold accelerations by ligand **B**.

Computational Studies of Mixed Aggregation. ^6Li and ^{15}N NMR spectroscopic studies reveal two limiting behaviors. Monodentate ligand **A** and hindered chelating ligand (η^1-bound) **C** afford mixed aggregated dimers and trimers ($\mathbf{12}_{A,C}$ and $\mathbf{13}_{A,C}$, respectively). Conversely, strongly chelating amino ether **B** forms exclusively mixed dimer $\mathbf{12}_B$. We calculated mixed aggregates of Me_2NLi and $H_2C{=}C(OLi)OMe$. A considerable body of computational data on the solvation of mixed dimers and trimers is beyond the scope of this text and is archived in Supporting Information. Two simple observations attesting to the relationship of chelation and mixed aggregation are summarized in eqs 23 and 24. In agreement with experimental data, mixed dimer **26** is more stable than **25** by 3.7 kcal/mol *per Li* (eq 23). The trans stereochemistry (placing the MeO and Me_2N moieties proximate) is preferred by 1.3 kcal/mol/Li. Moreover, chelation promotes mixed dimer **26** relative to mixed trimer **27** (eq 24).

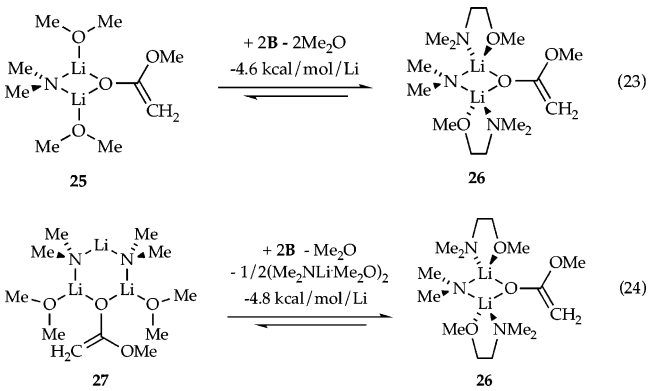

Computational Studies on Mixed Aggregate-Derived Enolizations. The rate studies of enolizations mediated by mixed dimer $\mathbf{12}_B$ are consistent with the competing monomer- and mixed dimer-based transition structures $[(i\text{-}Pr_2NLi)(\mathbf{B})(ester)]^{\ddagger}$ and $[(i\text{-}Pr_2NLi)(enolate)(\mathbf{B})_2(ester)]^{\ddagger}$, respectively. Accordingly, we focused on monomer-based transition structure **28**, dimer-based transition structures **29**−**31** that differ in the location hapticity of ligand **B**, and triple ion-based transition structure **32**.[37] The relative energies of activation are arbitrarily normalized to mixed dimer **26**. Disolvated structures containing a transannular contact could not be located presumably owing to steric hindrance. The calculations predict that chelated monomer **28** is the most stable transition structure, followed closely by bischelated dimer **31** and monochelated dimer **29**. Chelation of the external lithium in **31** is highly stabilizing (>3 kcal/mol), whereas chelation of the internal lithium proximate to the amido fragment in **30** is not significantly stabilizing (<1 kcal/mol). Transition structure **32**, corresponding to an ion pair-based pathway, is enormously destabilized.[38,17c]

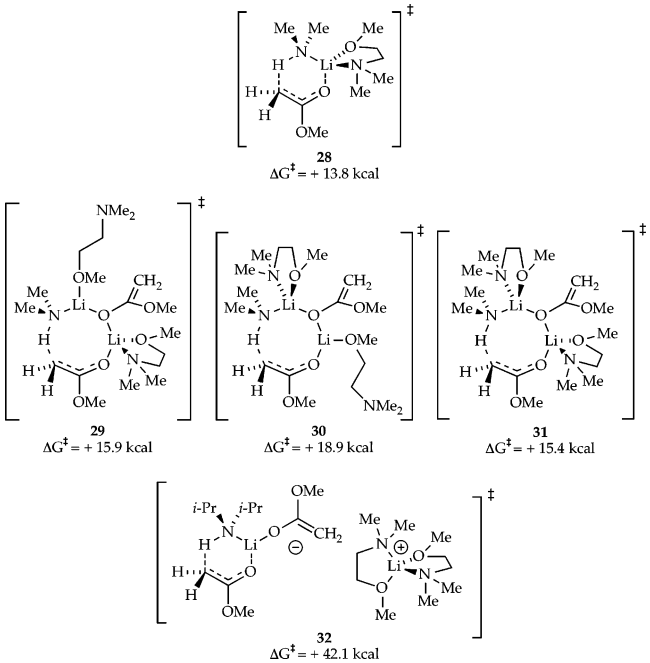

(35) For generic calculations on Li-amide mixed aggregates, see: (a) Pratt, L. M.; Lê, L. T.; Truong, T. N. *J. Org. Chem.* **2005**, *70*, 8298. (b) Pratt, L. M. *Minirev. Org. Chem.* **2004**, *1*, 209. (c) Pratt, L. M. et al. *J. Org. Chem.* **2003**, *68*, 6387. (d) Pratt, L. M.; Streitwieser, A. *J. Org. Chem.* **2003**, *68*, 2830. (e) Fressigné, C.; Maddaluno, J.; Marquez, A.; Giessner-Prettre, C. *J. Org. Chem.* **2000**, *65*, 8899. (f) Balamraju, Y.; Sharp, C. D.; Gammill, W.; Manuel, N.; Pratt, L. M. *Tetrahedron* **1998**, *54*, 7357. (g) McKee, M. J. *J. Am. Chem. Soc.* **1987**, *119*, 559.

(36) For a recent discussion on Li−H agostic interactions, see: Scherer, W.; McGrady, G. S. *Angew. Chem., Int. Ed.* **2004**, *43*, 1782, and references cited therein.

Scheme 1

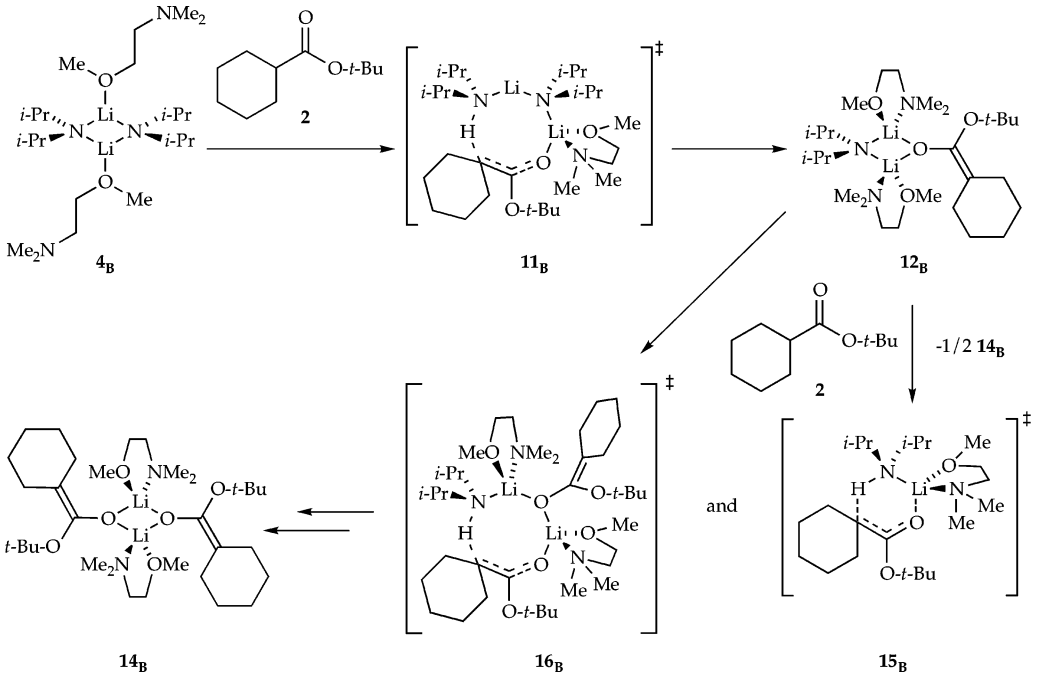

Discussion

Our attempts to understand the LDA-mediated enolization of ester **2** led to the structural and mechanistic scenario depicted in Scheme 1. We can now summarize the key observations and examine the origins of the ligand-*catalyzed* variant.

Hemilability and Dimer-Based Enolization. The sequence begins with disolvated dimer $\mathbf{4}_B$. A 10,000-fold acceleration by ≥1.0 equiv of amino ether **B** compared with analogous enolizations using *n*-BuOMe is attributable to hemilability—the penchant of amino ether **B** to bind as an η^1 (ether-bound) ligand in the reactant and as an η^2 (chelating) ligand in the transition structure. Although many LDA-mediated reactions are accelerated by **B**,[17] this example is the most striking reported to date.

Detailed rate studies (supplemented with analogous rate studies of the corresponding carboxamide enolization; eq 7) reveal that the enolization proceeds via a monoligated dimer-based transition structure: Computational, spectroscopic, and crystallographic evidence lends credence to the open dimer motif depicted in transition structure $\mathbf{11}_B$.[23−25] We are reminded[10,17b,19a,39] that mechanistic hypotheses based on presumed monomer-based reactivity may be oversimplified.

Autoinhibition. Many organolithium reactions require excess organolithium reagent to proceed to full conversion at appreciable rates. Indeed, enolizations using 1.0 equiv of LDA and excess ligand **B** stall at 50% conversion. Although a number of potential sources of autoinhibition were considered, we determined that the stalling in this instance derives from the quantitative formation of relatively unreactive mixed dimer $\mathbf{12}_B$. The mechanism by which mixed dimer $\mathbf{12}_B$ reacts makes for an interesting story.

Mixed Aggregate-Derived Enolization. Mixed aggregation effects on rates and selectivities were discussed as early as the 1960s.[40] $R_2NLi-LiX$ mixed aggregates appear to markedly influence the outcome of a number of synthetically important reactions of lithium amides, yet our understanding of them is remedial.[34,35] We first confronted mixed aggregation effects in Ph_2NLi alkylations in which autocatalysis was traced to the intervention of $Ph_2NLi-LiBr$ mixed aggregates.[41] Although semiquantitative studies of ester enolization[19b] and semiempirical computations[25b] have been used to probe the reactivities of $R_2NLi-LiX$ species, mechanistic details of reaction coordinates are sorely lacking.

We uncovered two pathways through which mixed dimer $\mathbf{12}_B$ reacts with ester **2**: (1) a mixed dimer-based enolization bearing two coordinated amino ethers as depicted in $\mathbf{16}_B$, and (2) a monomer-based enolization via transition structure $\mathbf{15}_B$ requiring dissociation (deaggregation) of the lithium amide and enolate fragments. Interestingly, the mechanism that demands dissociation of the enolate fragment provides the most interesting and unanticipated insights into mixed aggregation effects.

Enolization via mixed dimer $\mathbf{16}_B$ is shown to be prominent but much slower than that via LDA homoaggregated dimer $\mathbf{11}_B$. We showed that amino ether **B** is chelated in $\mathbf{11}_B$. Although we cannot confirm chelation of either of the two ligands in $\mathbf{16}_B$, DFT computations suggest that both of the amino ether ligands in transition structure $\mathbf{16}_B$ are bidentate. The strong affiliation

(37) A DFT study of mixed aggregates of Li bischelate $(LiS_4)^+$-enolate homoaggregates: (a) Yakimansky, A. V.; Müller, A. H. E. *J. Am. Chem. Soc.* **2001**, *123*, 4932. (b) Yakimansky, A. V.; Müller, A. H.; Beylen, M. V. *Macromolecules* **2000**, *33*, 5686.

(38) The ions included in transition structure **32** were fully optimized separately at the B3LYP/6-31G(d) level and the resulting structures were docked by approaching cation $(LiB_2)^+$ to the most accessible face of the anion. The only geometry constraints maintained along the optimization correspond to C−H and H−N bond distances intimately involved in the deprotonation.

(39) (a) Wiedemann, S. H.; Ramirez, A.; Collum, D. B. *J. Am. Chem. Soc.* **2003**, *125*, 15893. (b) Zhao, P.; Collum, D. B. *J. Am. Chem. Soc.* **2003**, *125*, 14411. (c) Zhao, P.; Collum, D. B. *J. Am. Chem. Soc.* **2003**, *125*, 4008. (d) Bernstein, M. P.; Collum, D. B. *J. Am. Chem. Soc.* **1993**, *115*, 8008.

(40) (a) *Ions and Ion Pairs in Organic Reactions*; Szwarc, M., Ed.; Wiley: New York, 1972; Vols. 1 and 2. (b) Szwarc, M. *Carbanions, Living Polymers, and Electron-Transfer Processes*; Interscience: New York, 1968. (c) Morton, M. *Anionic Polymerization: Principles and Practice*; Academic Press: New York, 1983. (d) *Anionic Polymerization: Kinetics, Mechanism, and Synthesis*; McGrath, J. E., Ed.; American Chemical Society: Washington D.C., 1981. (e) Cubbon, R. C. P.; Margerison, D. *Prog. React. Kinet.* **1965**, *3*, 403. (f) Roovers, J. E. L.; Bywater, S. *Macromolecules* **1968**, *1*, 328.

(41) DePue, J. S.; Collum, D. B. *J. Am. Chem. Soc.* **1988**, *110*, 5524.

among lithium enolate, lithium amide, and substrate in mixed dimer-based transition structure $\mathbf{16}_B$ offers an intuitively simple mechanistic model illustrating how extraneous lithium salts might influence reaction rates and product distributions.

For many years, we believed it to be a truism that extraneous lithium salts, whether explicitly added or generated during the reaction, cause pronounced changes in selectivity if, and only if, the salts are affiliated intimately with the organolithium reagent and substrate at the product determining transition structure. *This statement is wrong.* Whereas enolization beginning with LDA dimer $\mathbf{4}_B$ proceeds via dimer-based transition structure $\mathbf{11}_B$, enolization starting from mixed dimer $\mathbf{12}_B$ proceeds via the monomer-based transition structure $\mathbf{15}_B$. *Mixed aggregation markedly influences the relative efficacies of the LDA monomer- and homo-dimer-based pathways*. The influence of the free LDA concentration on the relative concentrations of transition structures $\mathbf{11}_B$ and $\mathbf{15}_B$ is illustrated in eq 25. In effect, quantitative mixed aggregation decreases the concentration of free LDA, affording a relative promotion of monomer-based transition structure $\mathbf{15}_B$.

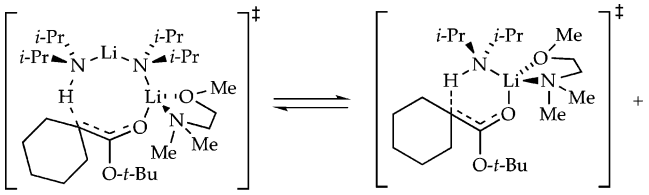

$\mathbf{11}_B$ $\mathbf{15}_B$

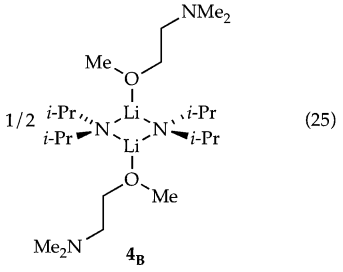

$\mathbf{4}_B$ (25)

The implications of this dilution effect are interesting and potentially important. Extraneous lithium salts can influence the mechanisms and, in turn, selectivities *without being intimately affiliated with the substrate or lithium-based reagent at the product-determining transition structure*.

Ligand-Catalyzed Enolization. We exploited the 10,000-fold acceleration imparted by ligand **B** to examine the principles underlying ligand-based catalysis. Initial efforts to catalyze the enolization by simply adding low concentrations of **B** failed because **B** binds tenaciously to mixed dimer $\mathbf{12}_B$. Monodentate ethereal cosolvents would not displace **B**. Consequently, we examined several ancillary ligands that might displace **B** from mixed dimer $\mathbf{12}_B$ without catalyzing the enolization. Indeed, stoichiometric quantities of amino ether **C** bearing a pendant *i*-Pr_2N moiety allow **B** to be used catalytically. Of course, ligand **C** is *more* precious than ligand **B**, but the point of this exercise is to demonstrate a proof-of-principle catalysis.

The cooperative effects of ligands **B** and **C** were unraveled via a combination of spectroscopic and computational studies. Chelating ligands are very sensitive to the steric demands of the ligand and the organolithium.[8,17] In the congested environment exemplified by LDA-dimer-based transition structure **11**,

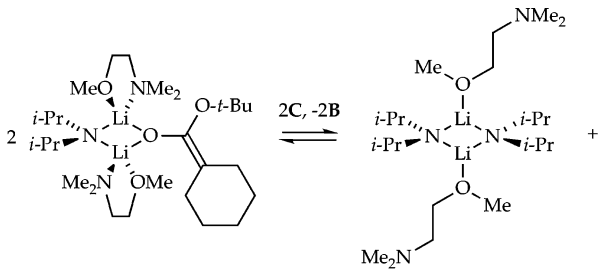

$\mathbf{12}_B$ $\mathbf{4}_B$

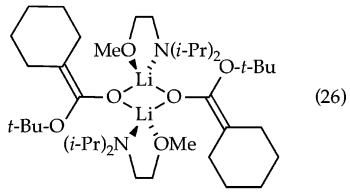

$\mathbf{14}_C$ (26)

replacing an Me_2N with a *i*-Pr_2N group almost totally precludes chelation. Indeed, ligand **C** displays little capacity to accelerate the enolization. We suspected that in the less congested environment of the mixed dimer $\mathbf{12}_B$, however, the differences between **B** and **C** would be attenuated, allowing for appreciable displacement of **B** by excess **C**. The structural studies suggest that the situation was somewhat more complex. Ligand **C** facilitates dissociation of **B**, but it does so by coordinating homoenolate dimer **14**, which in turn shifts the mixed aggregate-homoaggregate equilibrium as depicted in eq 26.

Conclusion

In the studies described herein, we dissected the seemingly simple enolization delineated in eq 6 into its components (Scheme 1). At the outset, dimer-based enolization dominates. As the reaction progresses, however, LDA-enolate mixed dimers become the prominent structural form, and the enolization diverts through both monomer-based and mixed dimer-based mechanisms. The monomer-based metalation, in particular, challenged a cherished notion about how mixed aggregation influences reactivity. The remarkable acceleration attributable to hemilability allowed us to develop a proof-of-principle ligand-based catalysis guided by structural, mechanistic, and computational data.

Although the structural and mechanistic scenario outlined in Scheme 1 appears to be exceptional, it is emblematic of the mechanistic complexity of organolithium chemistry. The harsh reality is that obtaining a mechanistic overview of a complete reaction coordinate demands considerable effort. It is not difficult to understand why progress toward understanding even the most generic organolithium reactions has been slow.

Acknowledgment. We thank the National Institutes of Health for direct support of this work and Merck, Pfizer, Boehringer-Ingelheim, R. W. Johnson, Aventis, Schering-Plough, and Dupont Pharmaceuticals (Bristol-Myers Squibb) for indirect support.

Supporting Information Available: NMR spectra, rate and computational data, experimental protocols, and complete refs 31, 35c. This material is available free of charge via the Internet at http://pubs.acs.org.

JA062147H